

## Selective Laser Sintering and Post-processing of Sisal Fiber/ Poly-(ether sulfone) Composite Powder

Jian Li,<sup>a</sup> Aboubaker I. B. Idriss,<sup>a,b,\*</sup> Yanling Guo,<sup>a</sup> Yangwei Wang,<sup>a</sup> Zhiqiang Zhang,<sup>a</sup> Hui Zhang,<sup>a</sup> and Elkhawad Ali Elfaki<sup>c</sup>

Selective Laser Sintering (SLS) technology can be utilized to recycle residues from forestry and agriculture, thereby alleviating shortages of materials and reducing energy consumption by producing wood-plastic pieces for industrial application. The mechanical strength of wood-plastic SLS parts is low, which restricts the application of this technology. In this study, a novel type of sisal fiber/poly-(ether sulfone) (PES) composite was prepared using a polymer mixing method in order to improve the mechanical properties of SLS parts. Single-layer sintering method was adopted to determine the proper processing parameters. The mechanical properties of the parts with different ingredient ratios and different particle sizes of sisal fiber before and after post-processing were tested using a universal testing machine. The morphology was examined using scanning electron microscopy (SEM). Results showed that the mechanical properties of the printed parts were relatively enhanced; when the mixing ratio of composite powder was 10/90 wt/wt. In addition, the part fabricated by powder of particles size less than 0.105 mm ( $0.125 \text{ mm} \geq \text{PS} < 0.105 \text{ mm}$ ) had the best mechanical strength. Moreover, the post-wax treatment significantly improved the strength of the parts, and the surfaces became smoother.

*Keywords:* Selective laser sintering; Sisal fiber flour; PES flour; Microstructure; Mechanical properties; Post-processing

*Contact information:* a: College of Mechanical and Electrical Engineering, Northeast Forestry University, Harbin 150040, China; b: Department of Mechanical Engineering, Faculty of Engineering Science, University of Nyala, Nyala, P.O. Box 155, Sudan; c: University of Bisha, College of Engineering, Mechanical Engineering Department, Bisha, Saudi Arabia, 61922 - Sudan University of Science and Technology, Department of Mechanical Engineering, College of Engineering, Khartoum, Sudan, 11113;

\* Corresponding author: aboubakerbolad@yahoo.com

### INTRODUCTION

Selective laser sintering (SLS), or laser sintering, is a type of additive manufacturing (AM) technology (Zeng *et al.* 2012; Guo *et al.* 2014). A modern technology combines computer-aided design, computer-aided manufacturing (CAD/CAM), computer numerical control (CNC), lasers, and materials science. This AM technology can be utilized to create 3D objects from a CAD model based on the principle of discrete accumulation (Guo *et al.* 2015; Bai *et al.* 2016; Yu *et al.* 2017). The SLS method was first reported by Williams and Deckard (1998). The principal advantage of SLS compared with other 3D printing technologies is the ability to create parts with enhanced geometric complexity and design flexibility without requiring expensive specific tooling (Lu and Reynolds 2008; Qi *et al.* 2017; Yu *et al.* 2018). Additionally, the parts made via SLS can have high precision and high mechanical properties. Furthermore, SLS technology does not require any support during manufacturing, and the produced

materials can be recycled (Yu *et al.* 2017). Therefore, SLS has generally been used in manufacturing, such as the automotive, aerospace, and construction industries, as well as for medical treatment (Mangano *et al.* 2013; Saboori *et al.* 2017). Recently, the development of materials for SLS mainly have been focused on metals, ceramics, polymers, and their corresponding composites (Gibbons *et al.* 2010; Yu *et al.* 2017, 2018; Aldahash 2018).

Material preparation technology is still commercially guarded, and the materials are quite expensive, which restricts the development and application of SLS (Zhao *et al.* 2017). Therefore, there is an urgent need to develop new natural and environmentally friendly materials with low cost, low energy consumption, and low CO<sub>2</sub> emission for SLS (Guo *et al.* 2015). Recently, several studies have been conducted to find an alternative cheap and environmentally friendly material to be used in AM processes. Yanling Guo and her team at Northeast Forestry University proposed a novel approach in the use of natural and cheap forestry waste as the feedstock of SLS to cut high material costs and environmental influence, and to additionally widen the scope of materials available for SLS (Guo *et al.* 2011). A number of previous studies focused on sintered wood-plastic composites (WPC) (Guo *et al.* 2011), rice husk powder/co-polyethersulfone (PES) (RHPC) (Zeng *et al.* 2012, 2013), walnut shell/Co-PES composite, and bamboo plastic composite. These previous studies exposed different physical and chemical properties, and these properties directly affect the forming performance of the composites.

Sisal fiber powder (SFP) is a biomass material. Compared to wood powder and rice husk powder, SFP is a substantial waste source and recyclable material, with a short growth cycle and large yield. Additionally, it conforms to the green design concept, with lower carbon emission and higher mechanical properties compared to wood powder. Based on the advantages of SFP, it has been selected as the structural material added to the PES matrix for developing a sisal fiber/PES composite (SFPC) as a feedstock for SLS. In this paper, the SFPC material was presented and sintered using SLS. The materials of this composite were carefully prepared with different mixture ratios (DMR) and different particle sizes (DPS) of SFP. The mechanical properties of SFPC were studied for three DPS and four DMR.

Additionally, the surface roughness value (SRV) was measured before and after post-wax treatment. The proposed DMR were 10/90, 15/85, 20/80, and 25/75(wt/wt), and the selected particle size range (PS) were (0.177 mm  $\geq$  PS < 0.149 mm, 0.125 mm  $\geq$  PS < 0.105mm, and 0.105 mm  $\geq$  PS < 0.093 mm). In this experiment the particle sizes passed through vibrating sieve were used to prepare SFPC, which are represent the particles size less than 0.149 mm, 0.105 mm, and 0.093 mm. To validate the mechanical properties a detailed comparison is presented between the tested specimens and related results in other research.

## EXPERIMENTAL

### Raw Materials

The raw materials studied in this experimental work were sisal fiber powder and PES powder. The sample of SFP shown in Fig. 1 (a) was provided as one of the ingredient materials for SFPC. The SFP was selected due to its high-density (1290 kg/m<sup>3</sup>), high tensile breaking force ( $2.55 \times 10^{-4}$  N), and low water content compared to other fibers. The PES is a type of thermoplastic polymer, as shown in Fig. 1 (b).

Importantly, it has stable, comprehensive performance modulus over a wide temperature range (-100 °C and 200 °C), and it has superior mechanical properties of the most thermoplastics materials, including ageing resistance (Knoell *et al.* 1999). Therefore, the SFP and polymer powder of PES were chosen as the main ingredients for preparing the SFPC material. The sisal fiber powder tended to make the composite more flexible and smoother. Also there were increases in the accuracy of dimensions of the SLS parts and it was possible to carry out treatments of the parts. The SFP was collected from Hangzhou Gaoke Composite Materials Co., Ltd. (Hangzhou, China), while the PES powder was collected from Shanghai TianNian Material Technology Co., Ltd. (Shanghai, China).

The SFP was dried to reduce the water content. First, the SFP was separated into size fractions using different mesh sizes of vibrating sieve to obtain the different particle sizes of SFP. In this experiment the particles size that passed through and the particles size collected on were expressed by the term of ( $X \geq PS < Y$ ). X is representing the particles size collected on and Y represents the particles size passed through the vibrating sieve. Therefore, the three different particle size of SFP were ( $0.177 \text{ mm} \geq PS < 0.149 \text{ mm}$ ,  $0.125 \text{ mm} \geq PS < 0.105$ , and  $0.105 \text{ mm} \geq PS < 0.093 \text{ mm}$ ), respectively. These ranges of particles size were obtained according to the American Standard (ASTM-E11). Then, the different size of SFP was put into the DHG-9140 electric heating thermostat drum (Long Yuan Technology Ltd., Beijing, China) and heated at 100 °C. To cut the water content (2% to 5%), the drying time was selected from 5 to 6 (hours). Finally, after completely drying powder, the sample was removed and cooled to prepare the composite material.

#### *Preparation process of sisal fiber/PES composite powder material (SFPC)*

The dried SFP was manually mixed with PES. The mixture ratios (MR) were categorized as 10/90 wt/wt, 15/85 wt/wt, 20/80 wt/wt, and 25/75 wt/wt, and the PS ranges selected were  $< 0.149 \text{ mm}$ ,  $< 0.105 \text{ mm}$ , and  $< 0.093 \text{ mm}$ , respectively. Then, the SFP and PES were mechanically mixed using an SHR-10A high-speed mixer (Hongji Machinery Ltd., Zhangjiagang, China) to attain a proper uniformity powder. The preparation processes of the SFPC are shown in Figs. 1 and 2. The SEM morphology of pure DPS sisal fiber powder (passed through) and PES powder are shown in Fig. 3

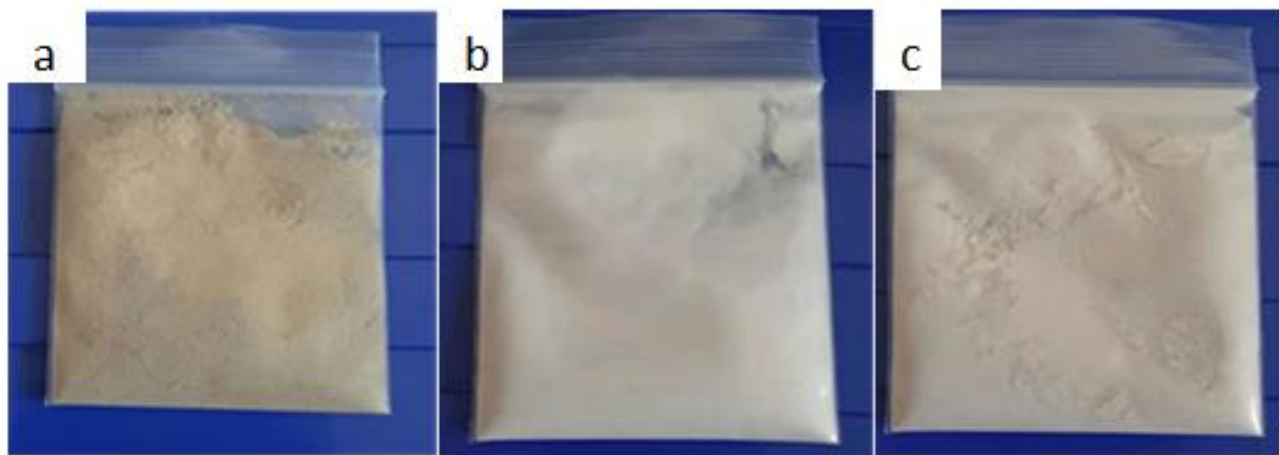


**Fig. 1.** (a) Sisal fiber powder (SFP); (b) PES powder; (c) sisal fiber/PES composites (SFPC)

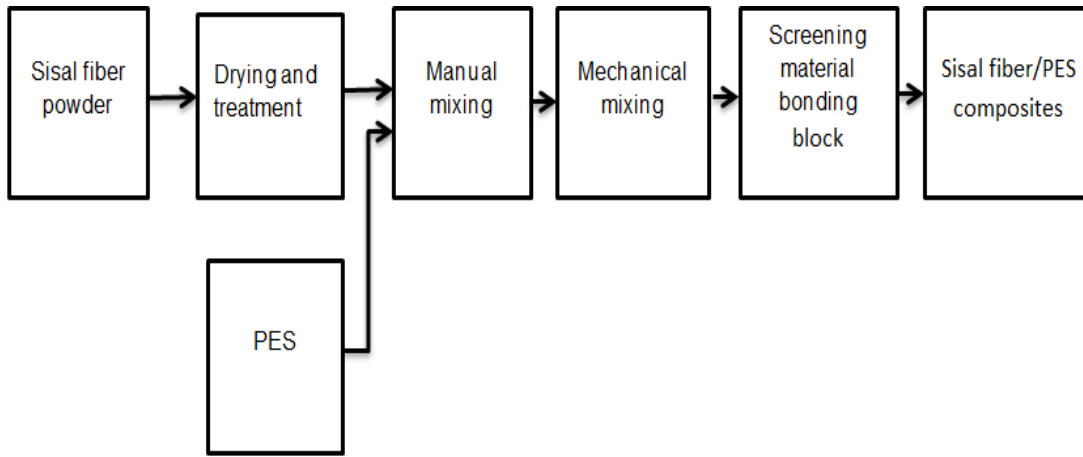


**Fig. 2.** Flow chart of the preparation process of sisal fiber/PES composites (SFPC)

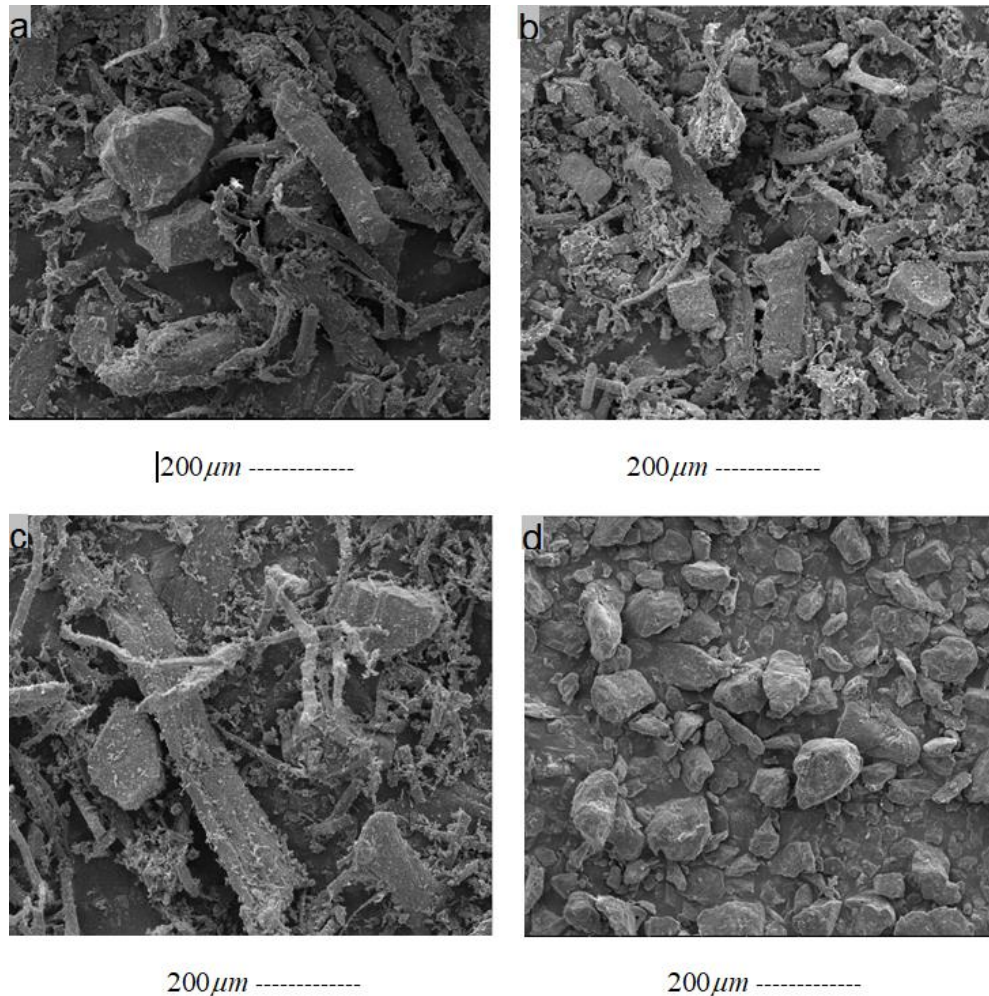


**Fig. 3.** SEM morphology of sisal fiber having particle size range (mm) less than (<0.149, <0.105 and <0.093) and PES; (a) sisal fiber, (<0.149); (b) sisal fiber, (<0.105); (c) sisal fiber, (<0.093); and (d) the PES

## Methods

### *SLS experiments*

The sintering process of the SFPC parts with different component proportions was conducted using an AFS-360 rapid prototyping machine made by the Beijing Longyuan Technology, Ltd. (Beijing, China). The equipment and building method are shown in Fig. 4. The main process parameters were as follows: scanning speed of 2000 mm/s, the layer thickness of 0.1 mm, scan spacing of 0.2 mm, laser power of 14 W, and preheating temperature of 82 °C. The processing temperature was 75 °C.

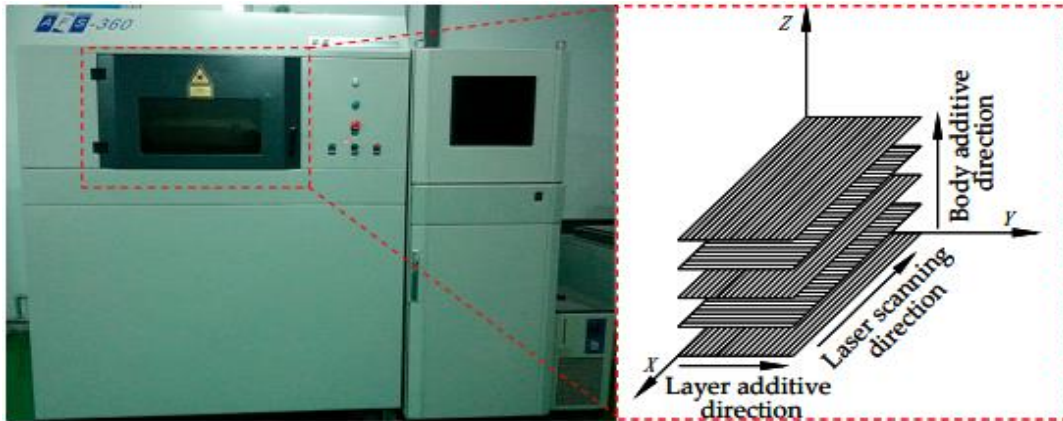


**Fig. 4.** AFS-360 rapid prototyping machine equipment and building method

### *Post-processing experiments*

The SFPC part was removed from the AFS-360, and the excess powder was cleaned carefully. Then, the cleaned part was placed in the electric heating thermostat drum at a temperature of 70 °C for 30 min. After completing the insulation, the part was slowly immersed in the wax pool. Finally, the waxing part was cleaned and prepared for the mechanical test. A post-processing flow chart of this experiment is shown in Fig. 5.

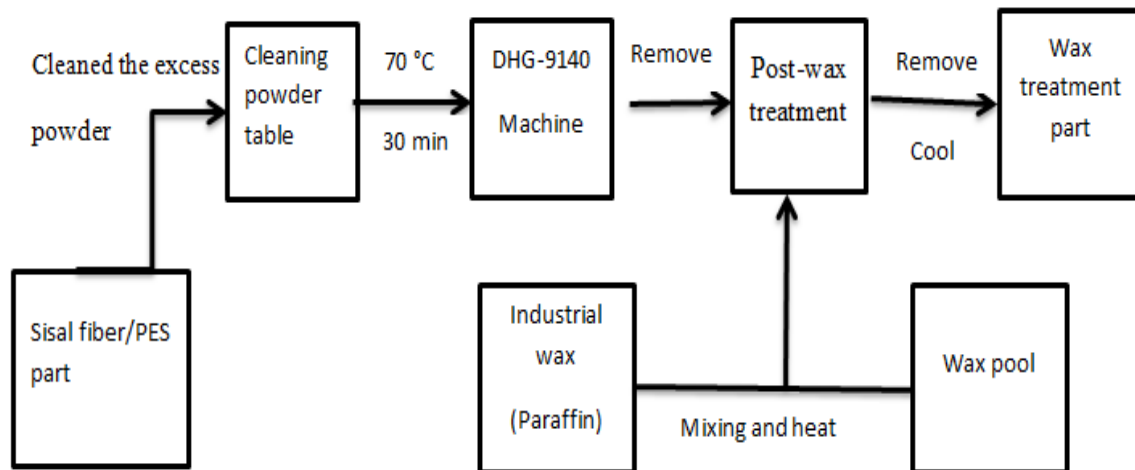


**Fig. 5.** The post-processing flow chart of sisal fiber/PES parts

### Scanning electron microscopy (SEM)

The SFP powder, PES powder and SFPC of different ingredient proportions were scanned using an FEI Quanta200 SEM (Dutch Company, Amsterdam, Netherlands). The morphology and the inner microstructures of the SFPC with DMR of (10/90, 15/85, 20/80 and 25/75) and DPS of SFP, within particle size ranges less than (<0.149 mm, <0.105 mm and <0.093), respectively, were obtained using the SEM device.

### Single-layer sintering experiment

Before the laser sintering experiment for the SFPC, a single layer sintering experiment was conducted to determine the feasibility of using the SFPC and the best ratio of the two main components. The SFPC samples were prepared based on the designed MR wt/wt of 10/90, 15/85, 20/80, and 25/75 and DPS of SFP. Each sample was manually deposited on a plate, and then the dish was placed in the middle of the part bed in an AFS-360 sinter station. Based on previous experience of sintering PES, the laser power was set at 14 W. The formula with the optimal content of SFP feasible for laser sintering was selected. Additionally, the raw materials were prepared for the subsequent laser sintering experiments.

### Mechanical test method

The mechanical tests of the specimens were conducted under atmospheric pressure. In this experiment, the bending strength test was performed via a three-point loading test. The STL format of the tensile specimens had dimensions of 150 mm × 20 mm × 10 mm, which was designed based on GB/T 1040 (1992). While the STL format of bending specimens had dimensions of 80 mm × 10 mm × 4 mm and was designed based on GB/T 9341 (2008). The bending strength was calculated according to Eq. 1,

$$\delta_f = \frac{3FL}{2bh^2} \quad (1)$$

where  $\delta_f$  is the bending strength (MPa),  $F$  is the force applied (N),  $L$  is the length (mm),  $b$  is the sample width (mm), and  $h$  is the sample thickness (mm). In the tensile test method, the static tensile load was adopted according to the properties of the machine test. The total length was 150 mm ± 0.5 mm, and the length of the middle parallel part was 60 mm ± 0.5 mm. The width of the middle parallel part was 10 mm ± 0.2 mm, the end width was 20 mm ± 0.2 mm, and the gauge length was 50 mm ± 0.5 mm. Additionally, the distance between the clamps was 115 mm ± 5 mm, the radius was 60 mm ± 0.5 mm, and the thickness was 4 mm ± 0.2 mm. The tensile strength was calculated using Eq. 2,

$$\delta_t = \frac{p}{bd} \quad (2)$$

where  $\delta_t$  is the tensile strength (MPa),  $p$  is the maximum load (N),  $b$  is the sample width (mm), and  $d$  is the sample thickness (mm). In this experiment, the mechanical properties of bending strength and tensile strength were conducted using the Byes-3003 microcomputer-controlled electronic universal testing machine (Jilin Province Taihe Ltd., Changchun, China). Each of the sample tests was measured three times, and then the average of the obtained data was taken the result, which is clearly shown in Tables 3 and 4. Additionally these tables include 95% confidence intervals for the means for lower and upper value. Figure 6 shows the sample test, in which Fig. 6a for the bending part test, Fig. 6b for the tensile part test, and Fig. 6c for the waxing part test.

## RESULTS AND DISCUSSION

### Single Layer Sintering Experiment

Through several single-layer sintering experiments, the suitable processing parameters of SLS for SFPC and PES were obtained. The preheating temperature of the chamber was between 70 °C to 86 °C, the laser power was between 10 W and 16 W, scan speed was between 1 m/s to 2.5 m/s, layer thickness was 0.1 mm, and scan spacing was 0.2 mm. To determine the optimum processing parameters, three groups of green parts of SFPC of 20/80 (wt/wt) were fabricated by SLS under the above processing parameters. These groups of green parts, specimens for the bending test, specimens for the tensile test, and specimens for the waxing test are shown in Fig 6 (a, b, and c) respectively. In the process, the layer thickness (0.1 mm) and the scan spacing (0.2 mm) were constant, which stood for different laser powers, scan speeds, and different preheating temperatures. The results showed that the optimum process parameters of SFPC were 82 °C preheating temperature, 14 W laser power, 2000 mm/s scan speed, 0.1mm layer thickness, and 0.2 mm scan spacing at the same parameters of the PES.

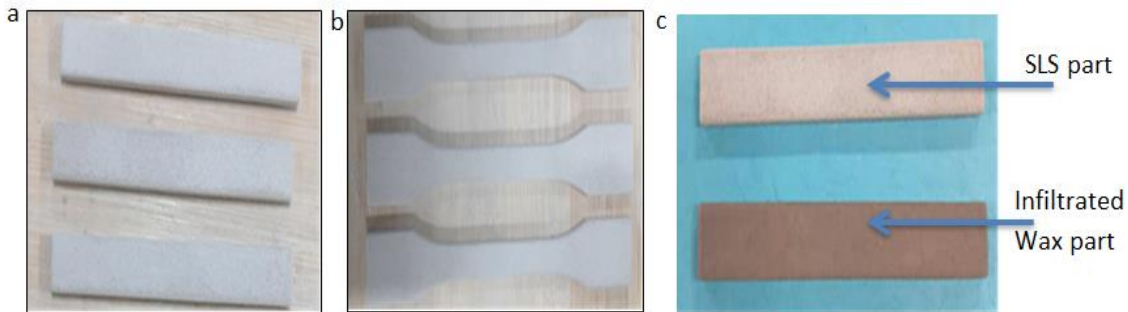
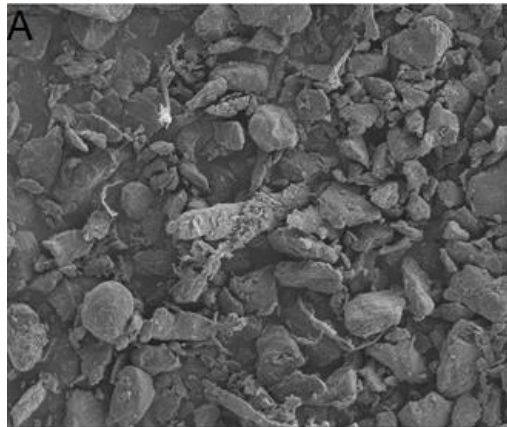


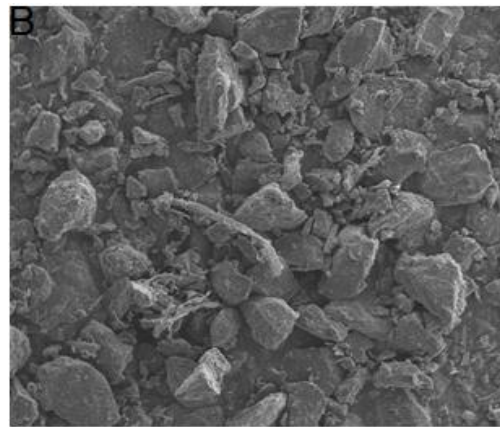
**Fig. 6.** Specimens prepared for (a) bending tests; (b) tensile tests; and (c) waxing tests

### Microstructure Analysis

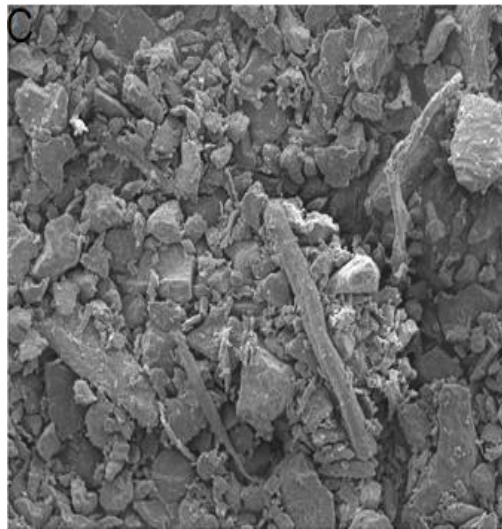
The morphology of sisal fiber powder at DPS less than ( $<0.149$  mm,  $<0.105$  mm and  $<0.093$  mm) and the PES powder were scanned using the SEM device, as shown in Fig. 3. Moreover the morphology of fracture surfaces specimens of DMR also was scanned via SEM. Figure 7(a, b, c, and d) shows the micro-morphology specimens of 10/90 15/85, 20/80 and 25/75 SFPC (wt/wt). Figure 7 explains the inner sintering neck between the SFP and PES particles and also shows the porosity between them. From Figure 7 it is apparent that, when the amount of SFP powder in the SFPC increased, the flow ability of the PES and the number of sintering necks between powder particles became lower. Meanwhile, the porosity of the parts was increased due to the lower density. Thus, the strength of SFPC part was reduced as a result of the density reduction by addition sisal fiber powder in SFPC. Therefore, the specimens of 10/90 wt/wt and 15/85 wt/wt had higher mechanical properties compared to other specimens of the SFPC. Figure 7, parts (e) and (f); show the morphology of DPS of sisal fiber powder composite. When the particle size of SFP was reduced from  $<0.149$  mm to  $<0.105$  mm, the voids between SFP and PES powder were reduced. Moreover, the porosity of the part decreased. And when the link between the molten powders was increased, the density of parts and mechanical strength were increased, which is clearly discussed in the mechanical properties section.



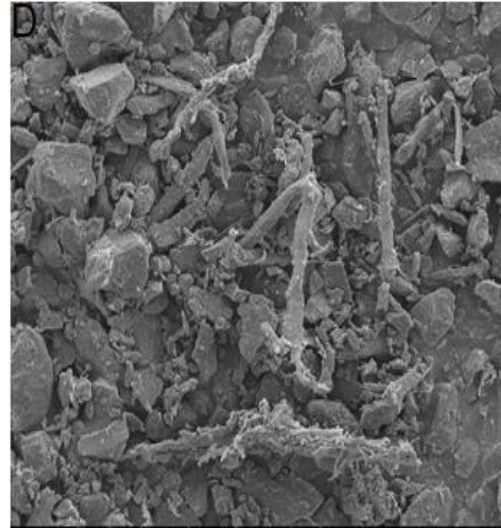
200 μm -----



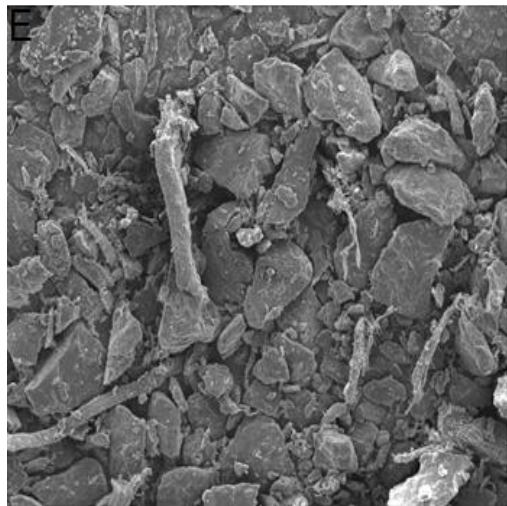
200 μm -----



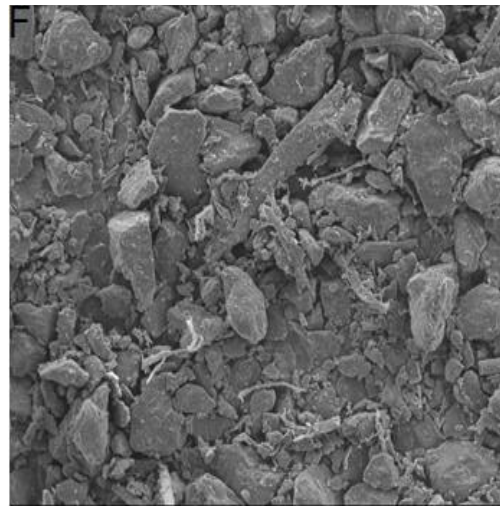
200 μm -----



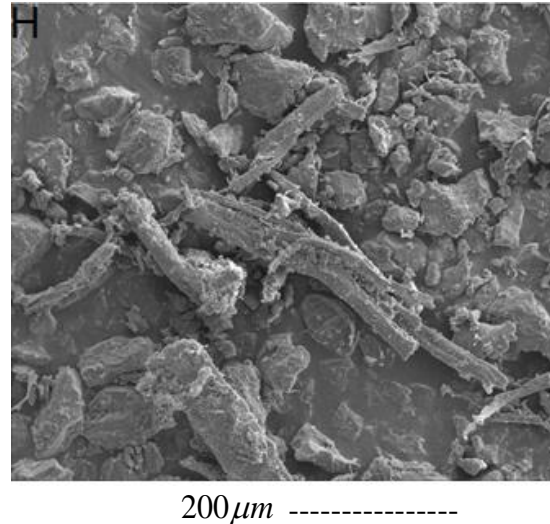
200 μm -----



200 μm -----

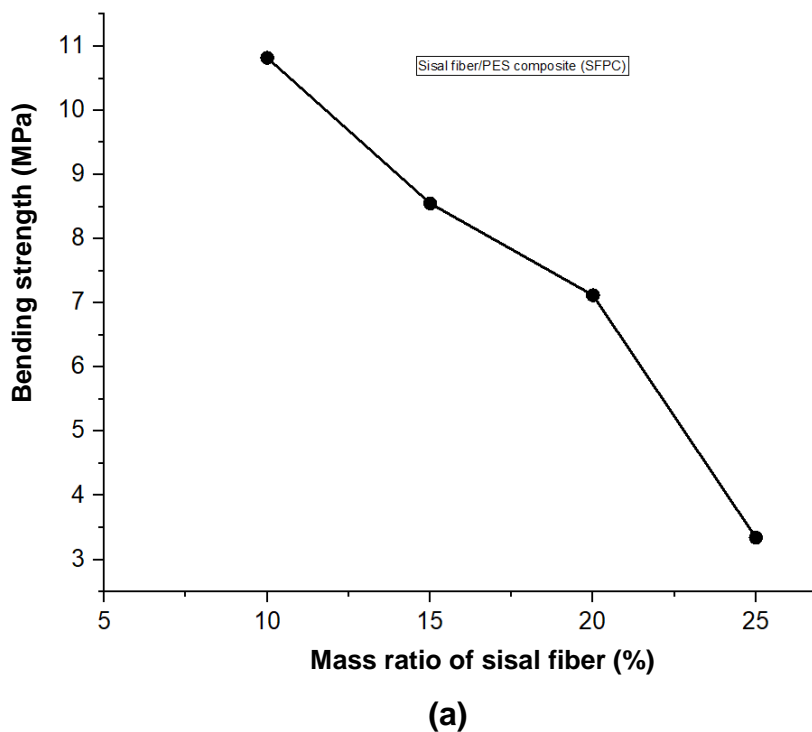


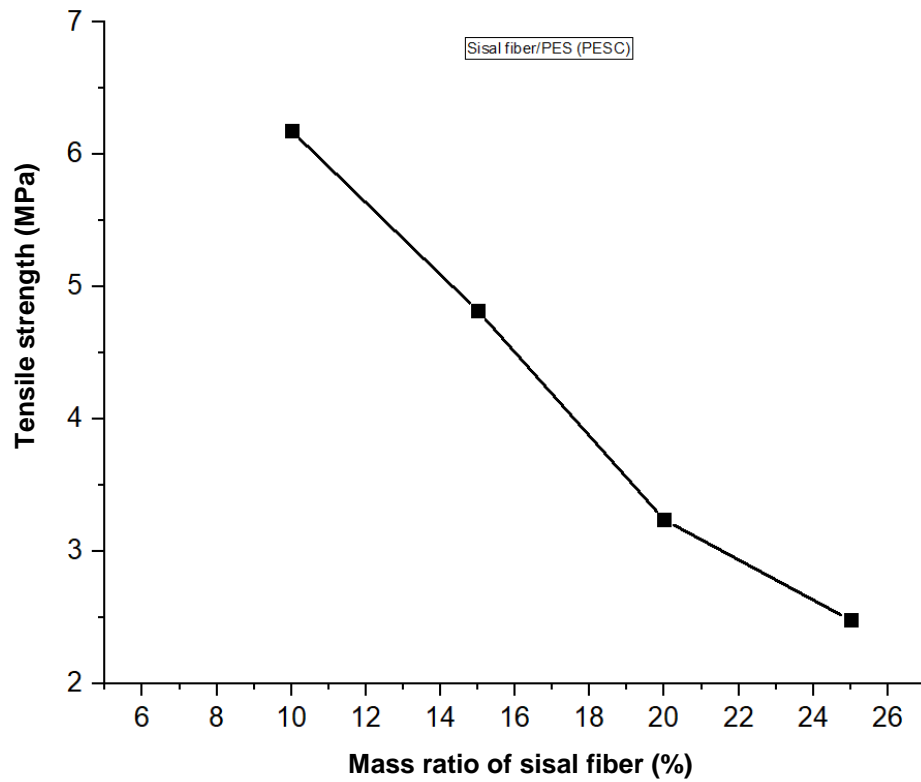
200 μm -----



**Fig. 7.** Morphologies of the DMR and DPS of the sisal fiber/PES composite. (a) sample of 10/90 SFPC; (b) sample of 15/85 SFPC; (c) sample of 20/80 SFPC; (d) sample of 25/75 SFPC; (e) represents the sample of SFPC at PS (<0.149 mm); (f) the sample of SFPC at PS (<0.105 mm); and (h) the sample of SFPC at PS (<0.093 mm) produced *via* SEM device.

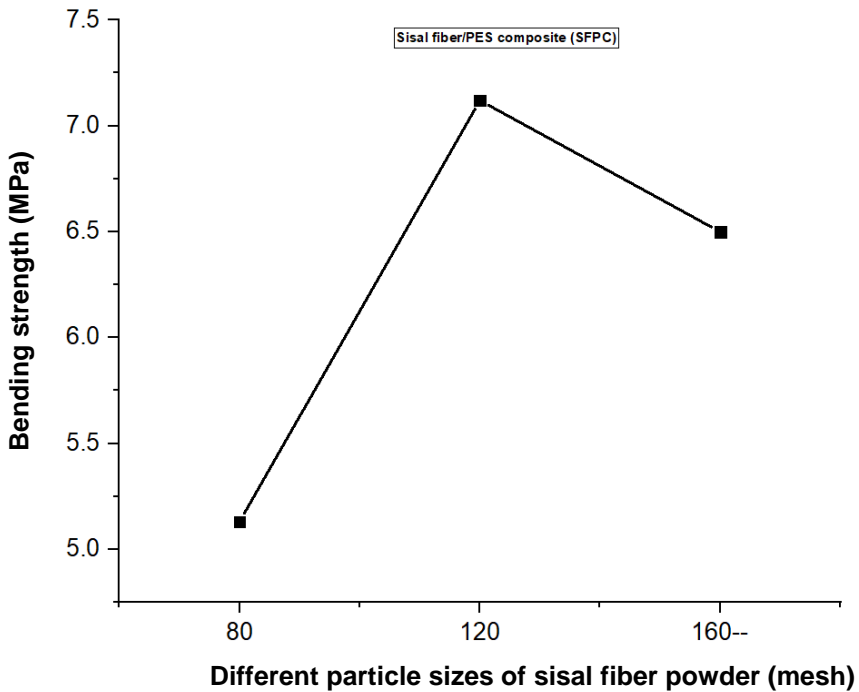
Since the particle sizes was increased, the density of the parts slightly declined, which resulted in a reduction in the strengths of the SLS parts. Similarly, when the PS reduced from <0.105 mm to <0.093 mm, the links between the molten powders of SFP and PES were reduced, which is shown in Fig. 7h. While the friction adhesion and surface forces between them were increased. Accordingly, the density and mechanical properties of the SFPC part significantly reduced. Finally, when the part is composed of particles having a size of <0.105 mm, the results were regarded as optimum, due to high density and strength.



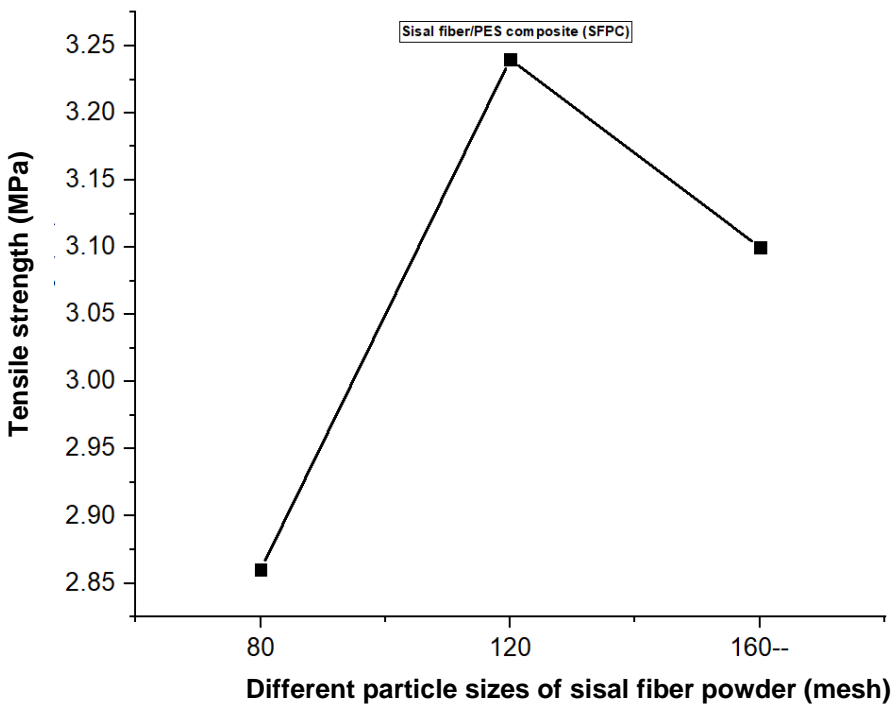


(b)

**Fig. 8.** Mechanical properties of sisal fiber/PES composite for different mixture ratios: (a) bending strength curves for different ratios; (b) tensile strength curves for different ratios



(a)



(b)

**Fig. 9.** Mechanical properties of sisal fiber/PES composite for different particle sizes: (a) Bending strength curves for different sizes; (b) tensile strength curves for different sizes

### Mechanical Properties

The specimens of 10/90, 15/85, 20/80, and 25/75 (wt/wt) MR and DPS of SFP (<0.149 mm, <0.105 mm and <0.093 mm) were fabricated in this experiment. The optimum parameters used for processing were as explained previously. The mechanical properties of bending strength and tensile strength of DMR are presented in Fig. 8. The results show that the average mechanical properties of green specimens of SFPC decreased with the increase in the content of sisal fiber powder. This was attributed to the decrease in density of the SLS part. The 10/90 part showed the highest mechanical properties among the DMR and better than the specimen of PES powder. The average mechanical properties of these are listed in Table 3. The cost of SFPC composite decreases with an increase in content of the sisal fiber powder. When the content of SFP in the composite was between 20/80 wt/wt and 25/75 wt/wt, the SLS part had the highest rate of decline in the bending strength, from 7.12 MPa to 3.34 MPa. Moreover, when the content was between 15/85 and 20/80, the specimens had the highest rate of the tensile strength decline, from 4.82 MPa to 3.24 MPa. The mechanical properties of the wood-plastic composite reported by Weiliang Zeng were relatively weak. The average mechanical strength of SFPC was remarkably higher than wood-plastic composite, which is listed in table 2.

Figure 9 shows the influence of the particle sizes relative to the mechanical properties of SLS parts. When the PS of SFP in the composite was (<0.149 mm), the bending and tensile strengths of sintered part were 5.13 MPa and 2.86 MPa, respectively.

When the PS was ( $<0.105$  mm), the strength was increased to 7.12 MPa and 3.24 MPa for bending and tensile, respectively. However, as the PS was became ( $<0.093$  mm), the mechanical strength of SLS parts slightly decreased due to low density of SLS part, which is clearly shown in Fig. 9 (a) and (b). Therefore, the part of PS ( $<0.105$  mm) was regarded as the optimum particle size in this experiment due to its superior mechanical properties. Table 1 shows the improvement value of the mechanical properties and surface roughness for the composite part before and after post-wax treatment. After polished the wax treatment part, the SRV became smoother due to the reduction of voids between SFP and PES powder. The SRV was measured via surface roughness tester device. The complex shape of SFPC provided by SLS is shown in Fig. 10. Parts (a) and (b) of the figure shows the complex shape before and after waxing treatment, respectively. A detailed comparison is presented in Table 2 between the tested specimens and the results reported in (Guo *et al.* 2011) to validate the mechanical properties of the tested specimens. The results showed that the mechanical properties of the current SFPC were significantly better than the results reported in the previous publication (Guo *et al.* 2011; Zeng *et al.* 2012). The potential applications of the developed sisal fiber/PES composites, it can be used in AM technology, such as furniture industry, wood composites, construction purposes, and the manufacture of carpets, rugs, ropes, *etc.*

**Table 1.** Comparison of Mechanical Strength and SRV of the SFPC before and After Post-wax Treatment

Parameter	SLS Parts Before Post-processing	SLS Parts After Waxing	Improvement Value %
Tensile strength (MPa)	3.24	4.12	27 %
Bending strength (MPa)	7.12	8.05	13 %
Roughness value (nM)	13.344	3.661	72 %

**Table 2.** Comparison of the Mechanical Properties between 20/80 wt/wt Sisal Fiber Composite and 20/80 wt/wt of Wood-plastic SLS Parts

Parameter	Stream Study	Guo <i>et al.</i> 2011
	Sisal fiber composite SLS part 20/80 wt/wt	Wood-plastic SLS part 20/80 wt/wt
Tensile strength (MPa)	3.24	2.17
Bending strength (MPa)	7.12	3.22

**Table 3.** Comparison of the average Mechanical Strength between DMR of SFPC and PES

Parts	Bending Strength Test Repeatability			Mean	95% confidence intervals for the means	Tensile Strength Test Repeatability			Mean	95% Confidence Intervals for the Means
	test 1	test 2	test 3			test 1	test 2	test 3		
PES	8.15	8.28	8.23	8.215	Lower =7.22 Upper=9.22	4.83	4.9	4.81	4.85	Lower =4.27 Upper=5.43
10/90	10.76	10.91	10.8	10.82	Lower =10.24 Upper=11.40	6.12	6.24	6.19	6.18	Lower =5.6 Upper=6.75
15/85	8.50	8.56	8.6	8.55	Lower=7.97 Upper=9.13	4.85	4.79	4.83	4.82	Lower =4.24 Upper=5.40
20/80	6.95	7.19	7.22	7.12	Lower=6.54 Upper=7.70	3.30	3.18	3.23	3.24	Lower=2.66 Upper=3.82
25/75	3.48	3.18	3.37	3.34	Lower=2.76 Upper=3.92	2.45	2.51	2.47	2.48	Lower=1.9 Upper=3.06

**Table 4.** Average Mechanical Strength of the Different Particle Size of SFPC

Parts (mm)	Bending Strength Test Repeatability			Mean	95% Confidence Intervals for the Means	Tensile Strength Test Repeatability			Mean	95% Confidence Intervals for the Means
	test 1	test 2	test 3			test 1	test 2	test 3		
<0.149 mm	5.17	5.2	5.03	5.13	Lower =4.55 Upper=5.71	2.83	2.85	2.9	2.86	Lower =2.28 Upper=3.44
<0.105 mm	7.06	7.14	7.17	7.12	Lower =6.54 Upper=7.70	3.27	3.25	3.2	3.24	Lower=2.66 Upper=3.82
<0.093 mm	6.3	6.7	6.5	6.5	Lower =5.92 Upper=7.08	3.12	3.15	3.04	3.1	Lower=2.52 Upper=3.68

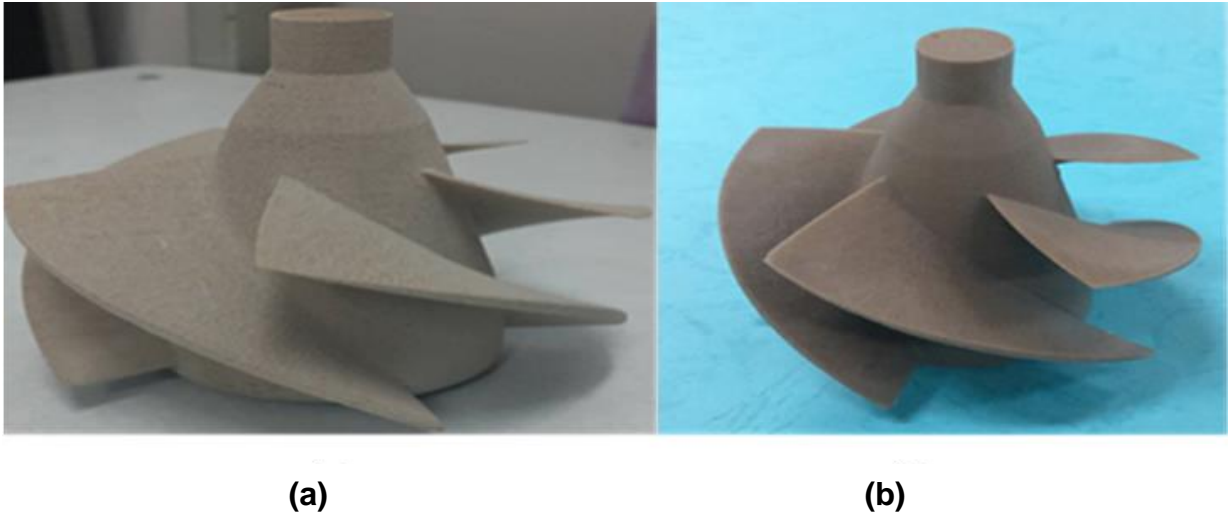


**Fig. 10.** Complex-shaped green parts of sisal fiber/PES composite provided by SLS: (a) SLS part before waxing; (b) SLS part after infiltrating waxing

## CONCLUSIONS

1. The sisal fiber/poly-(ether sulfone) (fiber/PES) composites could be sintered by selective laser sintering (SLS), thereby achieving high strength properties under suitable processing parameters.
2. The mechanical strength of green specimens of sisal fiber/PES composites decreased with the addition of sisal fiber powder. Thus, the mechanical strength of specimens of 10/90 wt/wt sisal fiber/PES composite was higher than those of 15/85 wt/wt, 20/80 wt/wt, and 25/75 wt/wt, and also higher than a part prepared with PES alone.
3. After post-wax treatment, the mechanical properties of green specimens of sisal fiber/PES composite for different moisture ratios (DMR) was remarkably improved, and the surface became smoother. The average tensile strength and bending strength were increased by 27% and 13%, respectively, and the surface roughness was significantly reduced to an optimum level after polished the wax part to 3.66 nM.
4. The mechanical properties of the sisal fiber/PES parts were affected by the particle size of sisal fiber. When the PS was  $<0.149$  mm, the curve of bending and tensile strength continuously increased until  $<0.105$  mm. Then, the bending and the tensile strength curve declined when the PS was less than  $<0.105$  mm.

## REFERENCES CITED

- Aldahash, S. A. (2018). "Optimum manufacturing parameters in selective laser sintering of PA12 with white cement additives," *Int. J. Adv. Manuf. Tech.* 96(1-4), 257-270. DOI: 10.1007/s00170-018-1584-y
- Bai, J., Zhang, B., Song, J., Bi, G., Wang, P., and Wei, J. (2016). "The effect of processing conditions on the mechanical properties of polyethylene produced by

- selective laser sintering,” *Polym. Test.* 52, 89-93. DOI: 10.1016/j.polymertesting.2016.04.004
- GB/T 1040 (1992). “Plastics- Determination of tensile properties,” Standardization Administration of China, Beijing, China.
- GB/T 9341 (2008). “Plastics- Determination of flexural properties,” Standardization Administration of China, Beijing, China.
- Gibbons, G. J., Williams, R., Purnell, P., and Farahi, E. (2010). “3D printing of cement composites,” *Adv. Appl. Ceram.* 109(5), 287-290. DOI: 10.1179/174367509X12472364600878
- Guo, Y., Jiang, K., and Bourell, D. L. (2014). “Preparation and laser sintering of limestone PA 12 composite,” *Polym. Test.* 37, 210-215. DOI: 10.1016/j.polymertesting.2014.06.002
- Guo, Y., Jiang, K., and Bourell, D. L. (2015). “Accuracy and mechanical property analysis of LPA12 parts fabricated by laser sintering,” *Polym. Test.* 42, 175-180. DOI: 10.1016/j.polymertesting.2015.01.019
- Guo, Y., Zeng, W., and Jiang, K. (2011). “Preparation and selective laser sintering of wood-plastic composite powder and post processing,” *Dig. J. Nanomater. Bios.* 6(3), 1435-1444.
- Knoell, T., Safarik, J., Cormack, T., Riley, R., Lin, S., and Ridgway, H. (1999). “Biofouling potentials of microporous polysulfone membranes containing a sulfonated polyether-ethersulfone/polyethersulfone block copolymer: Correlation of membrane surface properties with bacterial attachment,” *J. Membrane Sci.* 157(1), 117-138. DOI: 10.1016/S0376-7388(98)00365-2
- Lu, K., and Reynolds, W. T. (2008). “3DP process for fine mesh structure printing,” *Powder Technol.* 187(1), 11-18. DOI: 10.1016/j.powtec.2007.12.017
- Mangano, F., Bazzoli, M., Tettamanti, L., Farronato, D., Maineri, M., Macchi, A., and Mangano, C. (2013). “Custom-made, selective laser sintering (SLS) blade implants as a non-conventional solution for the prosthetic rehabilitation of extremely atrophied posterior mandible,” *Laser. Med. Sci.* 28(5), 1241-1247. DOI: 10.1007/s10103-012-1205-1
- Qi, F., Chen, N., and Wang, Q. (2017). “Preparation of PA11/BaTiO<sub>3</sub> nanocomposite powders with improved processability, dielectric and piezoelectric properties for use in selective laser sintering,” *Mater. Design* 131, 135-143. DOI: 10.1016/j.matdes.2017.06.012
- Saboori, A., Gallo, D., Biamino, S., Fino, P., and Lombardi, M. (2017). “An overview of additive manufacturing of titanium components by directed energy deposition: Microstructure and mechanical properties,” *Appl. Sci.* 7(9), Article Number 883. DOI: 10.3390/app7090883
- Williams, J. D., and Deckard, C. R. (1998). “Advances in modeling the effects of selected parameters on the SLS process,” *Rapid Prototyping J.* 4(2), 90-100. DOI: 10.1108/13552549810210257
- Yu, Y., Guo, Y., Jiang, T., Jiang, K., Li, J., and Guo, S. (2017). “Laser sintering and post-processing of a walnut shell/Co-PES composite,” *RSC Adv.* 37(7), 23176-23181. DOI: 10.1039/C7RA00775B
- Yu, Y., Guo, Y., Jiang, T., Li, J., Jiang, K., and Zhang, H. (2018). “Study on process and parameter optimization of selective laser sintering of walnut shell composite powder,” *BioResources* 13(2), 3017-3029. DOI: 10.15376/biores.13.2.3017-3029

- Zeng, W., Guo, Y., Jiang, K., Yu, Z., and Liu, Y. (2012). "Preparation and selective laser sintering of rice husk-plastic composite powder and post processing," *Dig. J. Nanomater. Bios.* 7, 1063-1070.
- Zeng, W., Guo, Y., Jiang, K., Yu, Z., Liu, Y., Shen, Y., Deng, J., and Wang, P. (2013). "Laser intensity effect on mechanical properties of rice husk-plastic composite parts fabricated by selective laser sintering," *J. Thermoplast. Compos.* 26(1), 125-136. DOI: 10.1177/0892705712461520
- Zhao, D., Guo, Y., Jiang, K., and Zhang, H. (2017). "Preparation and selective laser sintering of bamboo flour/copolyester composite and post-processing," *J. Thermoplast. Compos.* 30(8), 1045-1055. DOI: 10.1177/0892705715616854

Article submitted: July 11, 2019; Peer review completed: September 2, 2019; Revised version received: December 2, 2019; Accepted: December 23, 2019; Published: January 8, 2020.

DOI: 10.15376/biores.15.1.1338-1353